



Supplement of

Impacts of snow data and processing methods on the interpretation of long-term changes in Baffin Bay early spring sea ice thickness

Isolde A. Glissenaar et al.

Correspondence to: Isolde Glissenaar (isolde.glissenaar@bristol.ac.uk)

The copyright of individual parts of the supplement might differ from the article licence.

SUPPLEMENTARY MATERIALS

S1. Radar snow redistribution

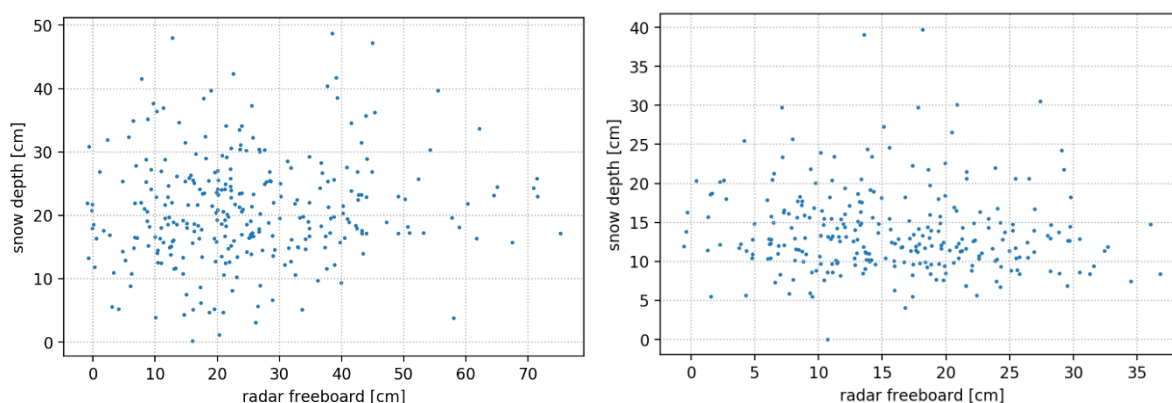
The sigmoidal function (Kwok & Cunningham, 2008) and the piecewise function (Petty et al., 2020) were designed to redistribute snow depth for high-resolution laser altimetry data. However, snow depth redistribution schemes have not yet been developed for radar altimetry data. Snow redistribution functions may be more appropriate for laser altimetry data because the measurements inherently contain the snow depth (total freeboard = snow depth + ice freeboard) or because of the generally higher resolutions. For radar altimetry data sets, a redistribution function can be found if snow depth is in some way related to ice freeboard only. Thus, we assess whether there is any benefit in using a radar freeboard snow redistribution scheme. We follow the methods outlined in Kurtz et al. (2009) to evaluate this, using Operation IceBridge data.

We assessed whether there is any benefit in using a snow redistribution scheme on radar freeboard data. We follow the methods outlined in Kurtz et al. (2009) to evaluate this, using Operation IceBridge data.

IceBridge L4 sea ice freeboard, snow depth, and thickness (version 1) data was obtained for the Arctic Ocean from 12 flights over 2 campaigns: April 2009 and March-April 2010 (Kurtz et al., 2015). The flights cover both multi-year ice and first-year ice regions. The total freeboard was obtained with the ATM instrument (Studinger, 2013) and the snow depth with the Snow Radar instrument (Paden et al., 2014).

Radar freeboard was estimated by subtracting the Snow Radar derived snow depth and a correction for light propagation speed through the snowpack from the ATM total freeboard. The propagation speed correction was applied using the spatially constant snow density from Kwok & Cunningham (2008). The airborne data was divided into 100 km sections, and the radar freeboard and snow depth were averaged over both the footprint scale of Envisat (2 km) and CryoSat-2 (300 m). A total of 133 sections were analysed.

The radar freeboard estimates did not show a relation with the snow depth on the length-scale of the pulse-limited footprint of the Envisat or the SAR-focused footprint of CryoSat-2 radar altimeters (Figure S1). This shows that snow redistribution on radar altimetry freeboard data would not improve the conversion from ice freeboard to thickness.



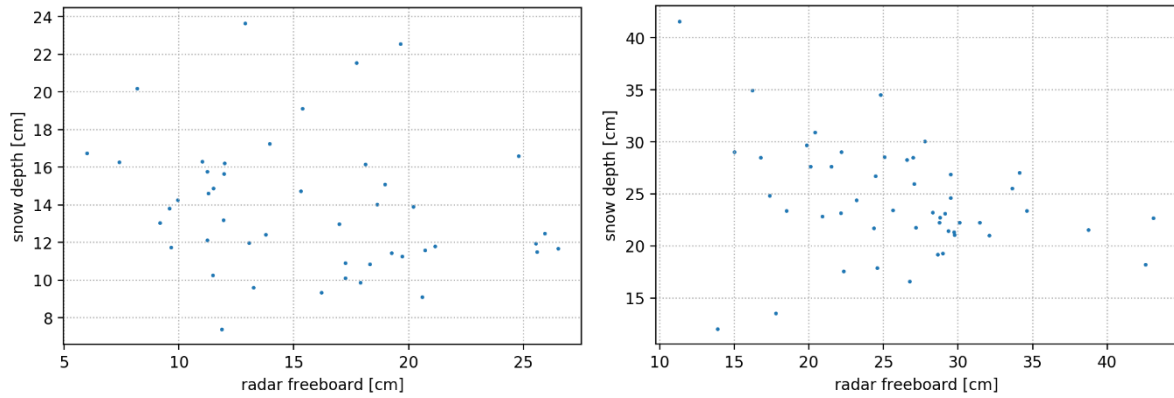


Figure S1. Four example 100 km sections of estimated radar freeboards and Snow Radar derived snow depths on the CryoSat-2 footprint length scale (300m) (top left, top right) and on the Envisat footprint length scale (2km) (bottom left, bottom right).

S2. March sea ice thickness from multiple processing methods

The ICESat March mean sea ice thickness (2003–2009) with all snow depth and density products and redistribution methods (Figure S2) show a similar pattern of thicker sea ice in the west of Baffin Bay compared to the east of Baffin Bay. A thinner region of sea ice is also observed in the northern part of the bay, where the North Water Polynya is known to exist. The W99 snow depth results in generally thicker sea ice than the PMW and the SnowModel-LG products. The W99 snow depth product results in generally thicker sea ice in the south of Baffin Bay, whereas the SnowModel-LG product results in thicker ice in the northern part of the bay. This product does not find thinner ice in the North Water Polynya region. Redistribution of snow along the sigmoidal function results in thicker sea ice, whereas redistribution along the piecewise function results in similar mean sea ice thickness as no redistribution. The application of the SnowModel-LG snow density results in thinner sea ice than the W99 snow density, but gives a similar spatial distribution.

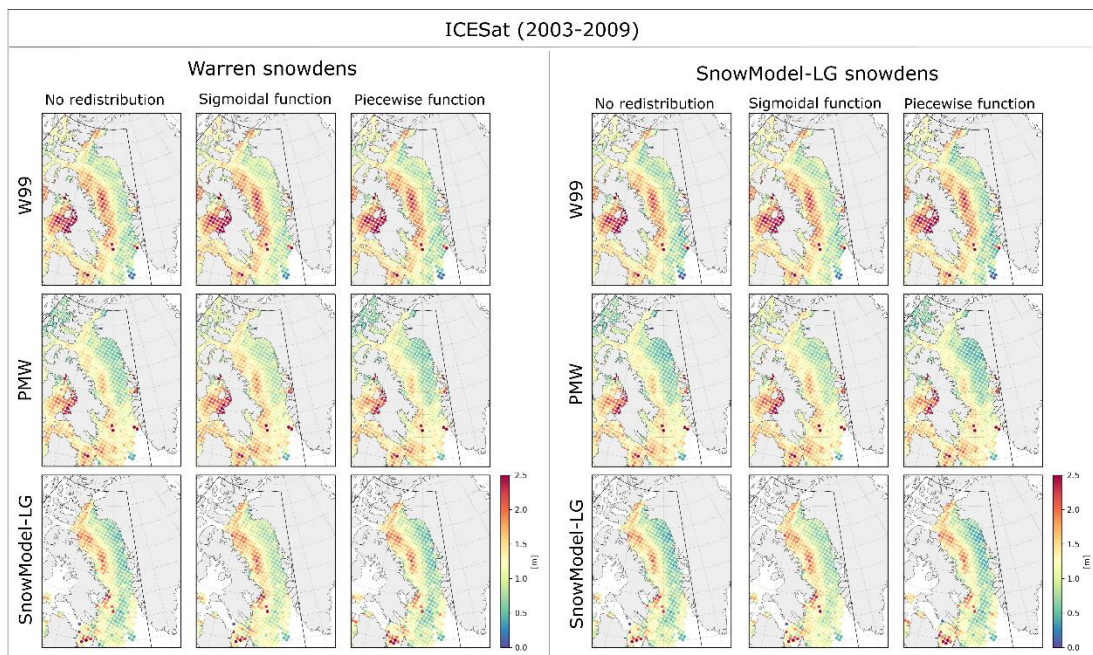


Figure S2. March mean sea ice thickness from ICESat (2003-2009) for all snow depth and density products and snow redistribution methods. The mean values are given in Table 2 (in the main paper).

Table S1. ICESat March mean sea ice thickness (2003-2009) for different snow depth products and snow redistribution methods. The first figure is with the W99 snow density value and the italic figure is with the SnowModel-LG snow density product.

	W99	PMW	SnowModel-LG
No redistribution	1.23 ± 0.45 m	1.03 ± 0.45 m	1.12 ± 0.44m
	<i>1.18 ± 0.49 m</i>	<i>0.98 ± 0.49 m</i>	<i>1.07 ± 0.49 m</i>
Sigmoidal function	1.28 ± 0.44 m	1.17 ± 0.45 m	1.22 ± 0.44 m
	<i>1.23 ± 0.49 m</i>	<i>1.10 ± 0.49 m</i>	<i>1.17 ± 0.49 m</i>
Piecewise function	1.24 ± 0.45 m	1.02 ± 0.45 m	1.12 ± 0.45 m
	<i>1.19 ± 0.49 m</i>	<i>0.94 ± 0.49 m</i>	<i>1.07 ± 0.49 m</i>

The CryoSat-2 sea ice thickness was determined with two radar freeboard products, the LARM product and the CCI product (which was used to compare with the Envisat CCI sea ice thickness). The CCI product is only available for the period 2011-2017, so we compare the processing methods for this period. The selected snow depth product has a large effect on the sea ice thickness found with CryoSat-2 (2011-2017) (Figure S3). The mean sea ice thickness is higher with the PMW snow depth product than the W99 snow depth, and even higher with SnowModel-LG (Table S2). Moreover, the found spatial distribution of sea ice thickness is dependent on the used snow depth product. The PMW snow depth product gives a strong west-east asymmetry in Baffin Bay, with thicker sea ice in the west of the bay. The SnowModel-LG snow depth product results in a thicker sea ice thickness strip along the east coast of Baffin Bay and thicker sea ice at the ice edge. The snow density product from SnowModel-LG results in generally thinner sea ice than the snow density from W99. The biggest difference in processing methods results from the applied radar freeboard product. The CCI product has thicker freeboards than the LARM product, and thus results in thicker sea ice thickness (~22%).

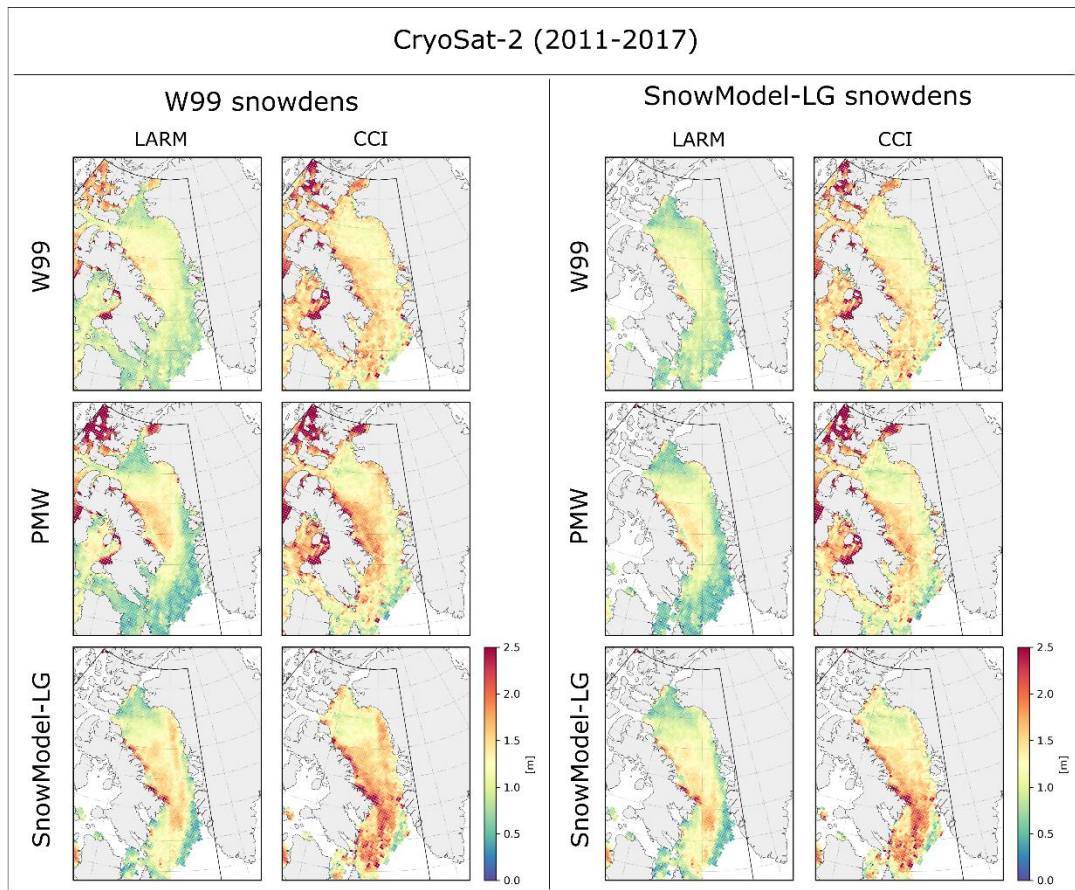


Figure S3. March mean sea ice thickness from CryoSat-2 (2011-2017) for all snow depth and density products and two radar freeboard products (LARM and CCI).

Table S2. CryoSat-2 March mean sea ice thickness (2011-2017) for different snow depth products and freeboard products. The first figure is with the W99 snow density value and the italic figure is with the SnowModel-LG snow density product.

	W99	PMW	SnowModel-LG
LARM	1.13 ± 0.43 m <i>1.02 ± 0.48 m</i>	1.19 ± 0.44 m <i>1.08 ± 0.49 m</i>	1.26 ± 0.44 m <i>1.14 ± 0.49 m</i>
CCI	1.38 ± 0.40 m <i>1.30 ± 0.45 m</i>	1.44 ± 0.40 m <i>1.34 ± 0.46 m</i>	1.45 ± 0.40 m <i>1.38 ± 0.46 m</i>

We also utilized snow depth estimates from the NASA Eulerian Snow On Sea Ice Model (NESOSIM) (Petty et al., 2018), which uses similar large-scale reanalysis and satellite data input to SnowModel-LG, but more simple parameterizations of snow accumulation and loss. NESOSIM snow depth estimates were applied as a second check on the effect of dynamic snow model results on sea ice thickness results in Baffin Bay. The March mean NESOSIM snow depth (Figure S4a) shows thicker snow depth in the west of Baffin Bay compared to the east. The NESOSIM snow depth also shows a lot thicker snow layer in the north of the bay compared to the other snow depth products (Figure 3), where the recurring North Water Polynya is located. The sea ice thickness from CryoSat-2 (LARM) with NESOSIM snow depth and W99 snow density (Figure S4b) provides slightly thicker sea ice in the west compared to the east, but the spatial distribution of sea ice thickness is more constant than with the other snow density products (Figure S3). The sea ice thickness in the north of Baffin Bay is thicker

with the NESOSIM snow depth product compared to the other snow depth products. The ICESat-2 sea ice thickness with NESOSIM snow depth (and piecewise redistribution) and the W99 snow density (Figure S4c) is comparable to the other snow depth products (Figure 5d) – with a strong west-east asymmetry – but shows thinner sea ice thickness in the north of the bay.

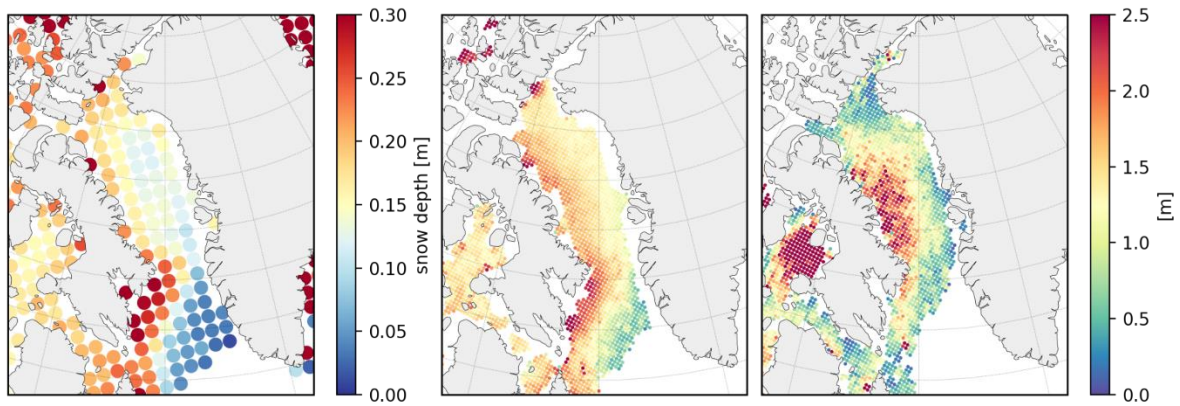


Figure S4. NESOSIM a) March mean snow depth (2010-2020), b) March mean SIT with CryoSat-2 LARM (2011-2020), and c) March mean SIT with ICESat-2 (2019-2020). Both sea ice thickness products were made with the W99 snow density and the snow depth on ICESat-2 was redistributed with the piecewise function.

S3. Satellite altimetry and ice charts

The estimated thickness and spatial patterns from the CIS ice charts are consistent with the ICESat and CryoSat-2 sea ice thickness results (Figure 8a). The mean thicknesses of ICESat and the CIS estimated thicknesses are 1.12 ± 0.47 m and 1.26 ± 0.26 m respectively, for the coinciding period of 2003-2009. The mean thicknesses of CryoSat-2 and the CIS thicknesses are 1.13 ± 0.47 m and 1.13 ± 0.26 m respectively, for the coinciding period of 2011-2020.

The stage of development from the CIS ice charts show strong agreement with the satellite altimetry sea ice patterns and offers the potential to be used as a proxy for the mean and regional distribution in sea ice thickness and spatial pattern.

The distribution of sea ice thickness from the overlapping CIS/ICESat and CIS/CryoSat-2 (Figure S5) periods are similar, although the CIS distributions are ‘peakier’ than the altimetry distributions implying the nine ice chart stages (Table 1) do not capture the full breadth of realistic ice stages of development.

The CIS ice charts do not seem to capture as much interannual variability as the satellite altimetry sea ice thickness products (Figure 6).

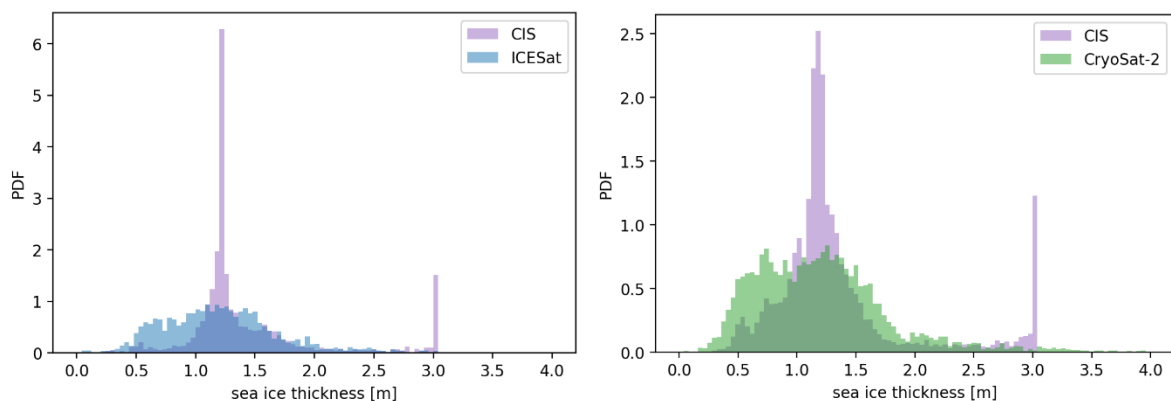


Figure S5. Distribution of sea ice thickness from CIS, ICESat and CryoSat-2

S4. Melville Bay

The CryoSat-2 sea ice thickness product shows a thick region in Melville Bay in the northeast of Baffin Bay in March for 7 of the 10 covered years (e.g. Fig. 7c). We have analysed surface roughness data retrieved by the radar altimeter, the length of the seasonal ice freezing period from the CIS charts, and the cumulative number of days after freezeup with air temperature above -5°C from ERA5 reanalysis data, within this region (Figure S6). Our results do not indicate that this thicker sea ice region in Melville Bay is caused by ice deformation or melt since the start of the freezing period. Years with thicker ice in the northeast region of the bay line up with years with thicker regional PMW snow depth. It is therefore plausible that the CryoSat-2 radar does not fully penetrate the snowpack in this area and therefore radar freeboards and thus sea ice thickness is overestimated. However, we did not find a relation between the number of snowmelt days after freeze-up and years with thicker sea ice estimates (i.e. suggesting partial radar penetration). Moreover, PMW snow depths for the greater Baffin Bay region closely resemble the depths estimated from ICESat-2 minus CryoSat-2 freeboards (Kwok et al., 2020) and produce very similar ice thickness results when applied to each sensor for 2019 and 2020. This implies CryoSat-2 is accurately retrieving the snow-ice interface elevation over most of the bay. Given the radar freeboards in this Melville Bay region do not reflect the interannual variations in PMW snow depth, i.e. thinner freeboards when depressed by thicker snow and vice versa, this finding may highlight a regional uncertainty in the PMW snow depths. The PMW depths may be overestimated in some years in this region, possibly owing to underlying sea ice conditions or a coastal effect we have not accounted for.

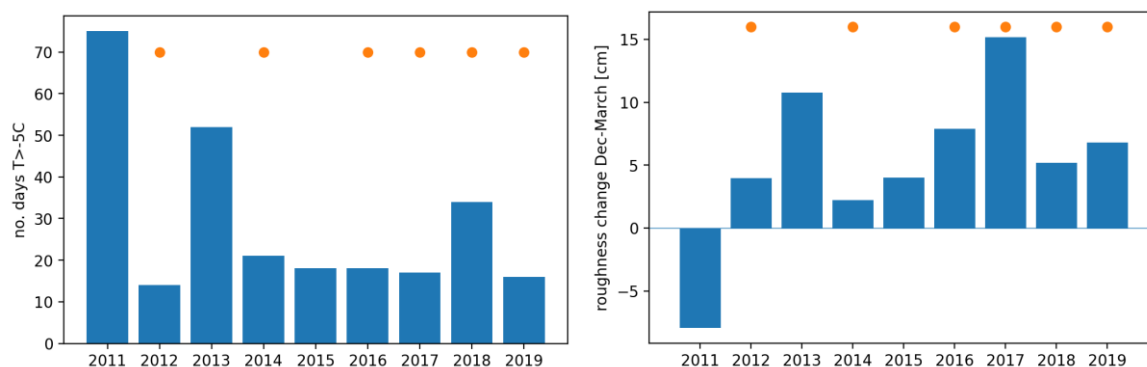


Figure S6. Left: number of days with surface temperature higher than -5°C since freezeup in Melville Bay from ERA5 reanalysis data (source). The orange dots show the years with thicker sea ice in Melville Bay. Right: sea surface roughness change between December and March

S5. Comparison sea ice thickness products

Since September 2004, a comprehensive observational program in Davis Strait has been providing sustained, long-term quantification of volume and freshwater transport between Baffin Bay and the Atlantic Ocean. As part of the program, Applied Physics Laboratory, University of Washington Mark 2 ULSs have been deployed to collect sea ice draft measurements along Davis Strait (Lee et al., 2004; Curry et al., 2014). The monthly mean draft and distribution at four locations in Davis Strait for 2006-2008 are available on http://psc.apl.uw.edu/sea_ice_cdr/Sources/Davis_Strait.html (Moritz).

The mean and standard deviation of ice draft from the ULS observations in March (Curry et al., 2014) was compared with the ICESat observations. The along-track ICESat sea ice thickness observations for all snow depth products and redistribution methods within 100 km of each of the ULS locations were retrieved. The ICESat draft (h_d) was determined by $h_d = h_i + h_s - h_f$, where h_i

is sea ice thickness, h_s is snow depth, and h_f is total freeboard (Figure 4). Only figures are shown with the SnowModel-LG snow density, as the results with the W99 snow density are very similar.

The observed mean draft from the ULS and the derived draft from the ICESat observations show general agreement (Figure S7). The ULS draft observations are on average thicker and have a larger standard deviation than the ICESat derived draft from all the processing methods (Table S3). The processing method from ICESat that shows most agreement with the mean draft from the ULS is the Warren '99 snow depth with sigmoidal snow redistribution. The draft observations from the ULS show, like the ICESat observations, generally thicker ice in the west of Davis Strait.

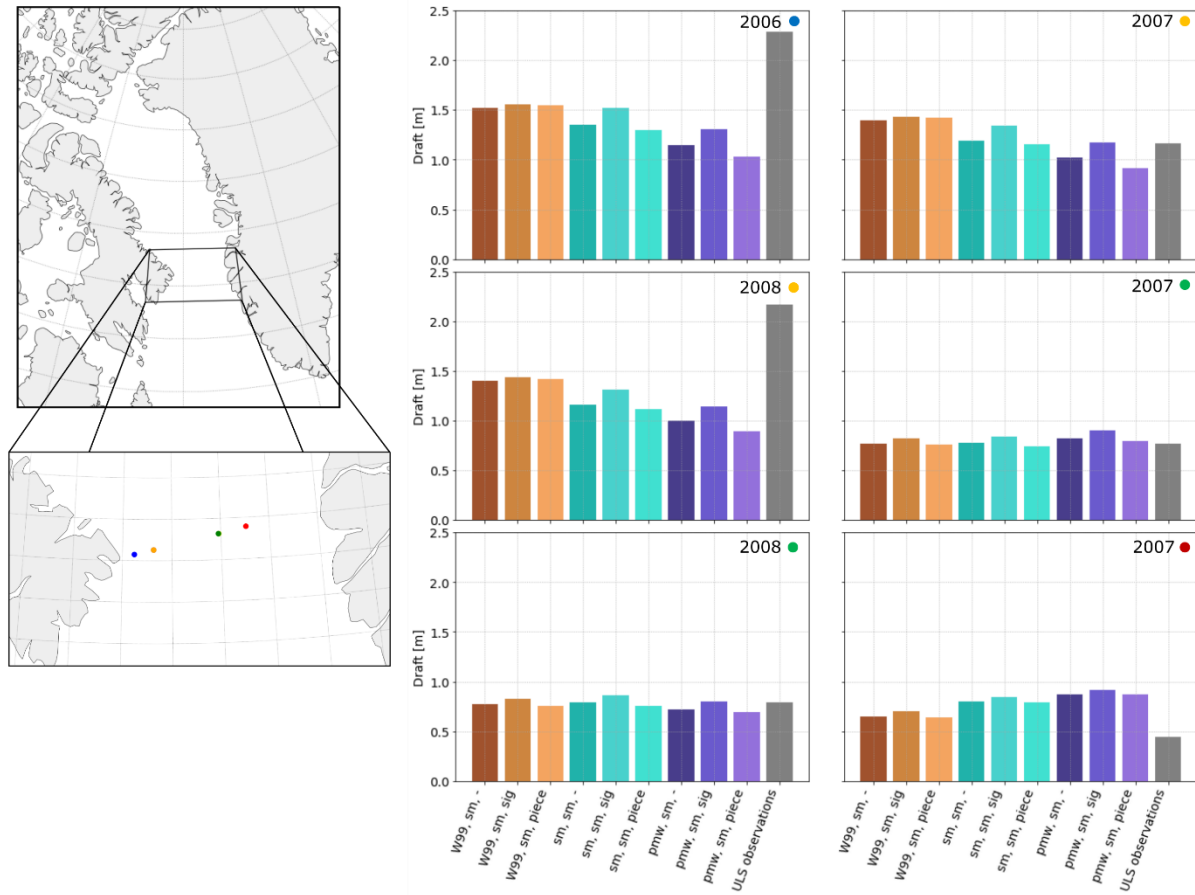


Figure S7. Mean draft from ULS observations at four locations in Davis Strait in grey (2006-2008) (Curry et al. 2014), compared to the corresponding sea ice draft from ICESat with all processing methods with SnowModel-LG snow density (snow depth product, snow density product, redistribution method). The colour in the top right of the panels corresponds with the location pointed out on the map.

Table S3. Mean difference between mean and standard deviation of ULS observed draft and ICESat draft (ULS-ICESat) from all snow depth products and redistribution methods (with SnowModel-LG snow density).

	Difference in mean	Difference in standard deviation
W99	0.18 ± 0.43 m	1.15 ± 0.75 m
W99 sigmoidal	0.14 ± 0.43 m	1.16 ± 0.75 m
W99 piecewise	0.18 ± 0.42 m	1.14 ± 0.74 m
PMW	0.26 ± 0.52 m	1.19 ± 0.77 m
PMW sigmoidal	0.15 ± 0.49 m	1.19 ± 0.76 m
PMW piecewise	0.29 ± 0.53 m	1.13 ± 0.72 m
SnowModel-LG	0.34 ± 0.61 m	1.20 ± 0.83 m
SnowModel-LG sigmoidal	0.23 ± 0.57 m	1.20 ± 0.80 m
SnowModel-LG piecewise	0.40 ± 0.65 m	1.19 ± 0.84 m

The mean sea ice draft distribution from the two western ULS locations was compared with coincident ICESat draft distribution of along-track observations within 100 km from the ULS locations for all ICESat processing methods (Figure S8). Statistical distribution comparison methods such as correlations, RMS difference, and the Kolmogorov-Smirnov statistic cannot be applied as we do not have the raw ULS draft measurements. Visually, the ICESat draft with the W99 and PMW snow depth products seem to capture the bimodal draft distribution that is visible in the ULS distribution, and show the best agreement for this location. The ICESat draft without snow depth redistribution seem to capture the very thin ice mode better, whereas applying a redistribution method results in better resolving the second, thicker mode.

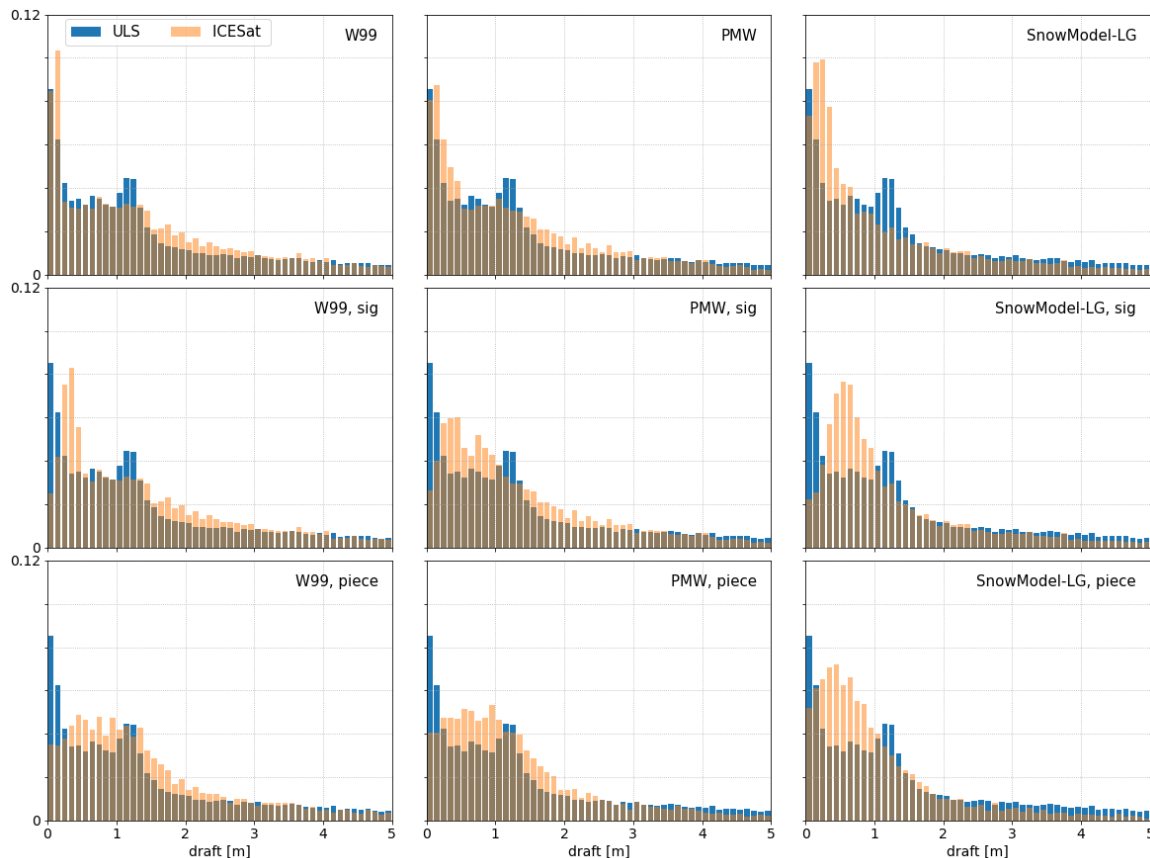


Figure S8. Mean sea ice draft distribution at western Davis Strait (2006-2008) (yellow and blue locations in Figure S7) from ULS and ICESat measurements for all ICESat processing methods with SnowModel-LG snow density.

The same methods were used to retrieve the distribution from ICESat for the two ULS locations in the east of Davis Strait (Figure S9). The draft is lower for both ICESat and ULS than in the west of Davis Strait, with shorter tails in the distribution. Again, the ICESat draft with the W99 and PMW snow depth products compare better with the ULS draft than the SnowModel-LG snow depth product, mostly for the thinnest drafts.

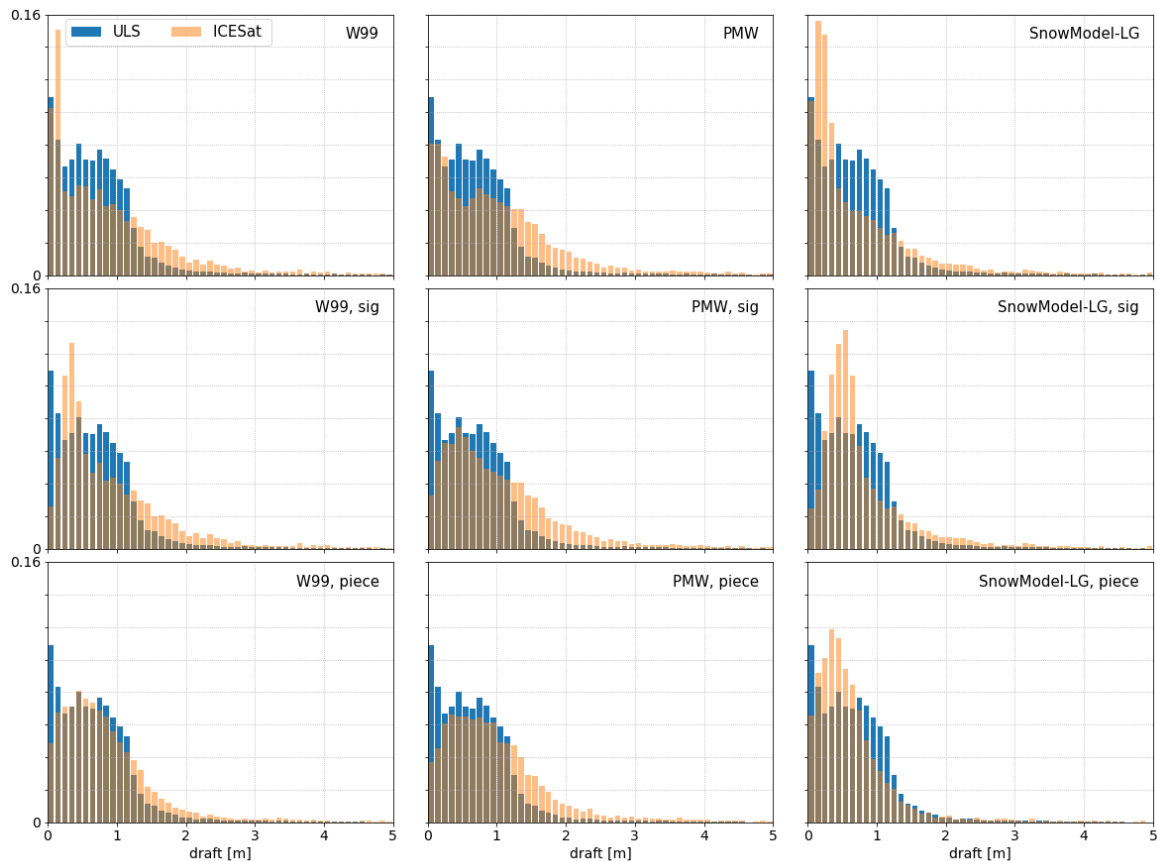


Figure S9. Mean sea ice draft distribution at eastern Davis Strait (2006-2008) (green and red locations in Figure S7) from ULS and ICESat measurements for all ICESat processing methods with SnowModel-LG snow density.

A comparison of the CryoSat-2 retrieved mean sea ice thickness with other sea ice thickness products over the same time-period shows comparable results. Figure S10 shows the ensemble mean sea ice thickness of three sea ice-ocean models and satellite observations by Min et al. (2021) for 2011-2016. This ensemble mean compares well with the CryoSat-2 sea ice thickness mean from all processing methods in this study. The spatial pattern of thicker sea ice in the south-west is similar. The CryoSat-2 SIT product shows thicker sea ice in the north-east of Baffin Bay.

The AWI CS2SMOS product (Ricker et al., 2017) shows generally thinner sea ice in Baffin Bay than the CryoSat-2 SIT product (Figure S11). The SMOS sensor is capable of measuring thinner sea ice than CryoSat-2, so integrating this product results in on average thinner sea ice thickness. However, the SMOS observations are known to systematically underestimate true sea ice thickness because ice thicker than 1 m cannot be measured, and the algorithm does not account for ice concentrations below 100% (Landy et al. 2017; Tian-Kunze et al., 2014). Combining CryoSat-2 and SMOS allows for measuring both thicker and thinner sea ice in the same region. Despite showing a general thinner sea ice cover, the spatial pattern is very similar to the CryoSat-2 product.

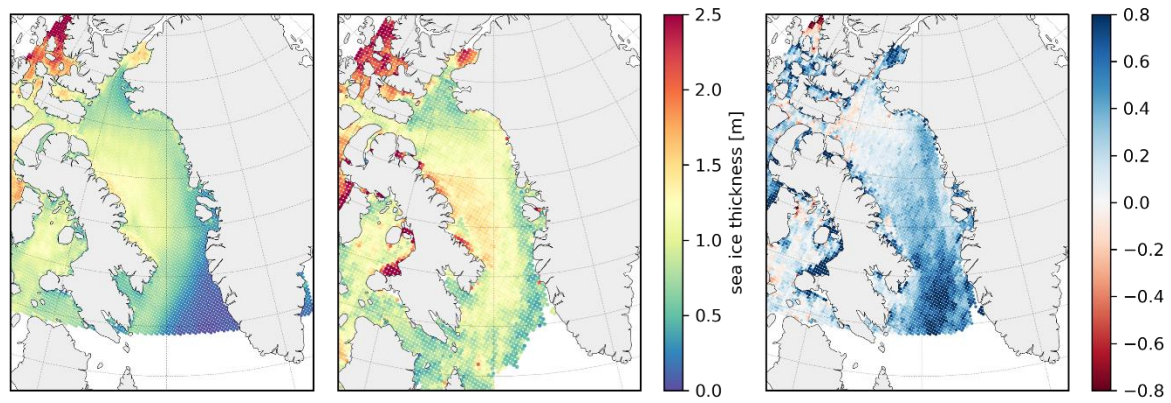


Figure S10. Left: The Min et al. (2021) ensemble mean sea ice thickness (m) in March averaged from CMST, NASOSIM, PIOMAS and Sat-merged SIT (2011-2016). Middle: CryoSat-2 mean sea ice thickness from all processing methods (2011-2016). Right: Difference CS2 mean SIT – Min et al. (2021) ensemble mean SIT.

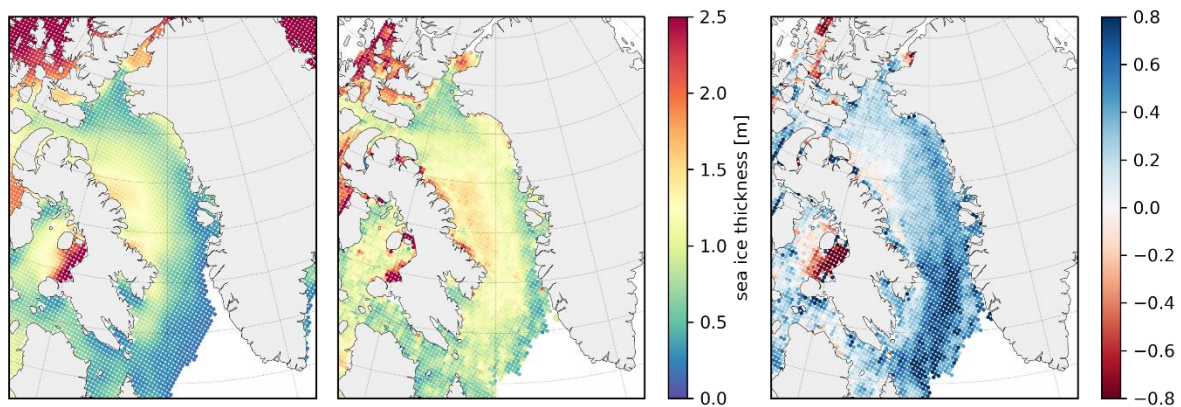


Figure S11. Left: AWI CS2SMOS sea ice thickness (2011-2020) (Ricker et al., 2017). Middle: CryoSat-2 mean sea ice thickness from all processing methods (2011-2020). Right: Difference CS2 mean SIT - AWI CS2SMOS.

References

- Curry, B., Lee, C.M., Petrie, B., Moritz, R.E., Kwok, R. (2014). Multiyear volume, liquid freshwater, and sea ice transports through Davis Strait, 2004-2010, *Journal of Physical Oceanography*, 44(4), 1244-1266.
- Kurtz, N., Markus, T., Cavalieri, D., Sparling, L., Krabill, W., Gasiewski, A. and Sonntag, J. (2009). Estimation of sea ice thickness distributions through the combination of snow depth and satellite laser altimetry data, *Journal of Geophysical Research: Oceans*, 114(10), 1-16.
- Kurtz, N., Studinger, M., Hareck, J., Onana, V. and Yi, D. (2015). IceBridge L4 Sea Ice Freeboard, Snow Depth, and Thickness, Version 1. Boulder, Colorado USA. NASA National Snow and Ice Data Center Distributed Active Archive Center. doi: <https://doi.org/10.5067/G519SHCKWQV6>.
- Kwok, R. and Cunningham, G. (2008). ICESat over Arctic sea ice: Estimation of snow depth and ice thickness, *Journal of Geophysical Research: Oceans*, 113(8), 1-17.
- Landy, J.C., Ehn, J.K., Babb, D.G., Thériault, N. and Barber, D.G. (2017). Sea ice thickness in the Eastern Canadian Arctic: Hudson Bay Complex & Baffin Bay, *Remote Sensing of Environment*, 200, 281-294.
- Lee, C.M, Petrie, B., Gobat, J.I., Soukhovtsev, V., Abriel, J., van Thiel, K., Scotney, M. (November 2004). An Observational Array for High-Resolution year-round measurements of volume, freshwater and ice flux variability

in Davis Strait: Cruise report for R/V Knorr 179-05, 22 September-4 October 2004. (Publication No.: APL-UW TR 0408). Applied Physics Laboratory, University of Washington. https://iop.apl.washington.edu/assets/pdfs/APL_UW_TR_0408.pdf

Min, C., Yang, Q., Mu, L., Kauker, F. and Ricker, R. (2021). Ensemble-based estimation of sea-ice volume variations in the Baffin Bay, *The Cryosphere*, 15(1), 169-181.

Moritz, R.E. Davis Strait Freshwater Flux Array, NSF Grant OPP-02300381. http://psc.apl.uw.edu/sea_ice_cdr/Sources/Davis_Strait.html

Paden, J., Li, J., Leuschen, C., Rodriguez-Morales, F. and Hale, R. (2014, updated 2019). IceBridge Snow Radar L1B Geolocated Radar Echo Strength Profiles, Version 2. Boulder, Colorado USA. NASA National Snow and Ice Data Center Distributed Active Archive Center, doi: <https://doi.org/10.5067/FAZTWP500V70>.

Petty, A.A., Webster, M., Boisvert, L. and Markus, T. (2018). The NASA Eulerian Snow on Sea Ice Model (NESOSIM) v1.0: Initial model development and analysis, *Geoscientific Model Development*, 11, 4577-4602.

Petty, A.A., Kurtz, N.T., Kwok, R., Markus, T. and Neumann, T.A. (2020). Winter Arctic sea ice thickness from ICESat-2 freeboards, *Journal of Geophysical Research: Oceans*, 125(5), 1-28.

Ricker, R., Hendricks, S., Kaleschke, L., Tian-Kunze, X., King, J. and Haas, C. (2017). A weekly Arctic sea-ice thickness data record from merged CryoSat-2 and SMOS satellite data, *The Cryosphere*, 11, 1607-1623, doi:10.5194/tc-11-1607-2017.

Studinger, M. (2013, updated 2020). IceBridge ATM L1B Elevation and Return Strength, Version 2. Boulder, Colorado USA. NASA National Snow and Ice Data Center Distributed Active Archive Center. doi: <https://doi.org/10.5067/19SIM5TXKPGT>.

Tian-Kunze, X., Kaleschke, L., Maaß, N., Mäkynen, M., Serra, N., Drusch, M., Krumpfen, T. (2014). SMOS-derived thin sea ice thickness: algorithm baseline, product specifications and initial verification, *The Cryosphere*, 8, 997-1018.